Analysis and Suppression of Circulating Harmonic Currents in a Modular Multilevel Converter Considering the Impact of Dead Time

Baichao Chen, *Member, IEEE*, Yaojun Chen, Cuihua Tian, Jiaxin Yuan, *Member, IEEE*, and Xiu Yao, *Student Member, IEEE*

***Abstract*—This paper focuses on analysis and suppression of circulating harmonic currents in a modular multilevel converter (MMC) considering the impact of dead time in medium-voltage applications. A continuous equivalent model of the MMC containing two ideal transformer models is presented. Using this model, the impact of a harmonic voltage upon the dc side is analyzed and the production mechanism of circulating harmonic currents is elucidated. At the same time, the impact of dead time and insulated gate bipolar transistor (IGBT) voltage drop (DTVD) is studied, which indicates that capacitor voltages, output harmonics, and circulating harmonic currents are influenced. Based on this analysis, an open-loop control strategy to suppressing circulating harmonic currents caused by the output current and DTVD is presented. Finally, all these conclusions are verified using a simulation platform with 14 modules per arm fed by a 14-kV dc voltage source and a downscaled experimental platform with four modules per arm fed by a 560-V dc voltage source.**

***Index Terms*—Circulating harmonic currents, dead time, equivalent model, excitation model, insulated gate bipolar transistor (IGBT) voltage drop, modular multilevel converter (MMC), open-loop control.**

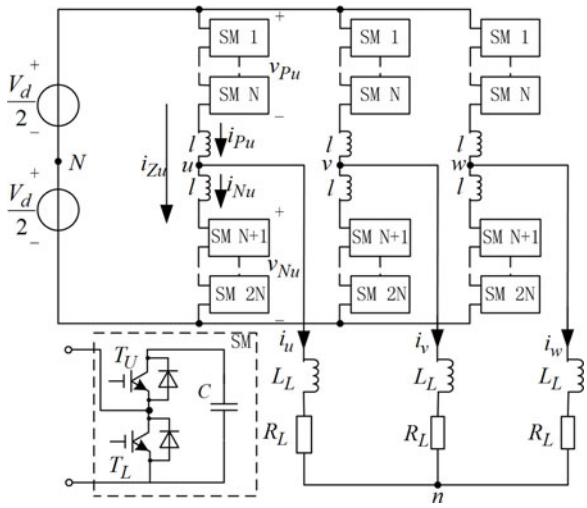

Fig. 1. Topology of the MMC.

I. Introduction

In medium- and high-voltage applications such as static reactive power compensation, motor drives, and high-voltage direct-current transmission, multilevel converters play an irreplaceable role and are widely used. Among these converters, the modular multilevel converter (MMC) has gained wide attention because of its outstanding advantages [1]–[7].

Lesnicar and Marquardt [8] introduced the basic concept and principle of this converter. The MMC topology, as shown in Fig. 1, consists of six arms, with N submodules in each arm. Thanks to its common dc bus, its modular structural design, and its simple realization of redundancy, this topology has gained wide attention, especially in the high-voltage direct-current transmission field. Other studies have addressed applications of MMCs for high-power motor drives and electric railway supplies [9], [10].

The existence of a circulating current between phases is an important property of the MMC, and therefore study of the circulating current and its harmonics is a hot topic, and many papers on this subject have been published. In [11] and [12], through solving the nonlinear differential equations for the inner variables, the harmonic components caused by the output current in the arm were described in depth, and analytical expressions for the harmonics were proposed. These analytical expressions indicate that the circulating harmonics influence each other, but this phenomenon was not analyzed comprehensively. In addition, in [11], it was proved that the circulating harmonic currents resonate at a particular frequency, but the derivation is very complex and cannot provide a clear physical concept. A continuous model characterized by the arm inductance, the arm resistance, and the resulting capacitance of all submodules when connected in series was proposed in [13] and [14] and was used in open-loop control for negative-sequence currents in dc transmission systems. In fact, this model is a low-frequency model that ignores the carrier frequency and is therefore suitable for study of external characteristics but not of internal ones. A frequency-domain MMC model was discussed in [15] and [16],

Manuscript received April 21, 2014; revised June 29, 2014; accepted August 2, 2014. Date of publication August 12, 2014; date of current version February 13, 2015. Recommended for publication by Associate Editor B. Lehman. *(Corresponding author: J. Yuan.)*

B. Chen and C. Tian are with the Wuhan University, Wuhan 430072, China (e-mail: whgycbc@163.com; 13886089037@163.com).

Y. Chen is with the Wuhan Electronic Information Institute, Wuhan 430010, China, and also with the School of Electrical Engineering, Wuhan University, Wuhan 430072, China (e-mail: cyj_cq@126.com).

J. Yuan was with the Wuhan University, Wuhan 430072, China. He is now with the Ohio State University, Columbus, OH 43210 USA (e-mail: yjx98571@163.com).

X. Yao is with the Ohio State University, Columbus, OH 43210 USA (e-mail: yao.110@osu.edu).

Color versions of one or more of the figures in this paper are available online at http://ieeexplore.ieee.org.

Digital Object Identifier 10.1109/TPEL.2014.2346957

in which the MMC was decoupled into an equivalent dc circuit and an equivalent ac circuit. However, the interaction between the ac and dc models was not analyzed.

For circulating current control, a phase-shift SPWM strategy was presented in [9], [17], and [18], in which each submodule was controlled by a subcontroller coordinated by a common controller to control the circulating current and the capacitor voltages. With this strategy, the circulating current can be controlled, but the control structure is very complex, and suppression of circulating harmonics is not perfect. In [19]–[21], an open-loop control strategy with prediction of the steady states of the system variables was implemented successfully to suppress circulating harmonic currents and to control capacitor energy. Using this strategy, only a few variables need to be measured, and the control effect is satisfactory. However, this strategy depends on the equivalent resistance in the arm, which shows nonlinear characteristics and cannot be valued precisely. Based on the analysis of the circulating harmonic currents in [11], to suppress every circulating harmonic current, each type of harmonic was addressed by an independent controller in [22], a strategy which ignored the causal relationships between the circulating harmonic currents and resulted in an excessive number of controllers. In [23], the dynamic characteristics of the dc bus were analyzed, and in [24], the overall system stability was investigated, but the process of exciting a harmonic voltage (which may come from the input dc voltage source, the internal control voltage, a change in capacitor voltage, or from other sources) on the dc side was not mentioned.

Moreover, previous studies of the MMC were mostly based on ideal power devices, ignoring dead time and insulated gate bipolar transistor (IGBT) voltage drop (DTVD). In high-voltage direct-current transmission, the switching frequency is very low and the output currents are very high, and therefore the impact of DTVD is not very significant. However, in medium-voltage applications, the number of submodules per arm is relatively small. To obtain low harmonic output voltage, the equivalent switching frequency has to be relatively high, and at the same time, the output current is probably not high, so the impact of DTVD becomes significant. Li *et al*. [25] argued that dead time would change the modulating rules of the system and improved the capacitor-voltage sampling strategy to reduce the impact of dead time, but how DTVD influenced the system was not analyzed. This paper focuses on the analysis and suppression of circulating harmonic currents considering the impact of dead time. The contributions are listed below:

An equivalent model of the MMC is introduced based on improving the expression of the equations presented in [23]. Using the model described earlier, the change process on any harmonic voltage on the dc side is described, and a causal relationship among circulating harmonic currents is proposed. Following this, the impact of DTVD upon the system is analyzed. Based on the production mechanism of circulating harmonic currents, the idea of suppressing circulating harmonic currents by eliminating their producing factors is proposed and used in the open-loop control strategy to suppress circulating harmonic currents caused by output current and DTVD. Unlike that described in [19]–[21], this strategy does not try to control capacitor energy, and it does not depend on the equivalent resistance in the arm. Finally, all the conclusions are verified using a simulation platform with 14 kV dc input and 14 submodules per arm and a downscaled experimental platform fed by a 560 V dc source with four submodules per arm.

II. Equivalent Model of the MMC

A. Assumptions and Basic Equations

During the analysis, the following assumptions are used:

1. the system is continuous, because of its multilevel output and high equivalent frequency, the harmonics in the output are minimal, and ignoring them would not affect the analysis;
2. the submodule capacitor voltages are balanced, that is, in the same arm, every submodule capacitor voltage is the same;
3. the upper and lower arms are symmetrical, including the modulation signal and the circuit parameters.

According to Kirchhoff's law, the following equations can be derived from the MMC circuit:

$$v_{uN} = \frac{1}{2}V_d - v_{Pu} - l\frac{di_{Pu}}{dt} - r_d i_{Pu} \tag{1}$$

$$v_{uN} = -\frac{1}{2}V_d + v_{Nu} + l\frac{di_{Nu}}{dt} + r_d i_{Nu} \tag{2}$$

where i_{Pu} and i_{Nu} are currents flowing through the upper and the lower arms, respectively, and r_d is the equivalent resistance in the arm. In Fig. 1, i_u is the load current and i_{Zu} is the circulating current, which exists in the circuit but cannot be detected directly. These currents satisfy the following equations [17], [18]:

$$i_{Pu} = \frac{1}{2}i_u + i_{Zu} \tag{3}$$

$$i_{Nu} = -\frac{1}{2}i_u + i_{Zu} \tag{4}$$

$$i_u = i_{Pu} - i_{Nu} \tag{5}$$

$$i_{Zu} = \frac{1}{2}(i_{Pu} + i_{Nu}). \tag{6}$$

By substituting (3)–(6) into (1) and (2), the following equations can be derived:

$$v_{uN} = \frac{v_{Nu} - v_{Pu}}{2} - \frac{1}{2}l\frac{di_u}{dt} - \frac{1}{2}r_d i_u \tag{7}$$

$$2l\frac{di_{Zu}}{dt} = V_d - (v_{Pu} + v_{Nu}) - 2r_d i_{Zu}. \tag{8}$$

According to the modulation rules, the voltages on the submodule stacks of the upper and lower arms can be expressed as

$$v_{Pu} = \frac{1 - S_u}{2}v_{Pu}^{\Sigma} \tag{9}$$

$$v_{Nu} = \frac{1 + S_u}{2}v_{Nu}^{\Sigma} \tag{10}$$

where $S_u = m_u \sin(\omega t + \varphi_u)$ is the modulation function of the u phase, with φ_u as the phase shift. The phase difference of

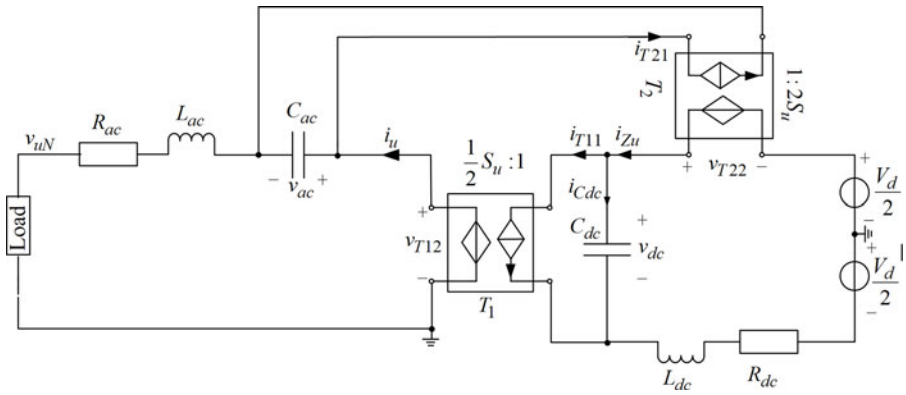

Fig. 2. Equivalent model of a single-phase MMC.

the three-phase modulation function is 120°. v_{Pu}^{Σ} and v_{Nu}^{Σ} are the sum of the capacitors in the upper and the lower arms, respectively.

B. Equivalent Model

According to power balance, the power consumed by the submodule stack is equal to the power sum of each submodule capacitor in the arm. Then the capacitor power in the submodule stacks of the upper and lower arms must satisfy the following equations:

$$v_{Pu}i_{Pu} = v_{Pu}^{\Sigma}C^{\Sigma}\frac{dv_{Pu}^{\Sigma}}{dt} \tag{11}$$

$$v_{Nu}i_{Nu} = v_{Nu}^{\Sigma}C^{\Sigma}\frac{dv_{Nu}^{\Sigma}}{dt} \tag{12}$$

where $C^{\Sigma} = C/N$. By adding and subtracting (11) and (12) and considering (3)–(10), the following expression can be derived:

$$\mathbf{Z}p\mathbf{x} = \mathbf{A}\mathbf{x} + \mathbf{B}\mathbf{u} \tag{13}$$

where p is the differential operator, $\mathbf{Z} = \text{diag}[L_{\text{dc}}\ L_{\text{ac}}\ C_{\text{dc}}\ C_{\text{ac}}]$, $\mathbf{x} = [i_{Zu}\ i_u\ v_{\text{dc}}\ v_{\text{ac}}]^T$, $\mathbf{u} = [V_d v_{\text{un}}]^T$

$$\mathbf{A} = \begin{bmatrix} -R_{\text{dc}} & 0 & -1 & 2S_u \\ 0 & -R_{\text{ac}} & \frac{1}{2}S_u & -1 \\ 1 & -\frac{1}{2}S_u & 0 & 0 \\ -2S_u & 1 & 0 & 0 \end{bmatrix}$$

$$\mathbf{B} = \begin{bmatrix} 1 & 0 \\ 0 & -1 \\ 0 & 0 \\ 0 & 0 \end{bmatrix}, \qquad C_{\text{dc}} = 2C^{\Sigma}$$

$$C_{\text{ac}} = 8C^{\Sigma}, \qquad v_{\text{dc}} = \frac{v_{Pu}^{\Sigma} + v_{Nu}^{\Sigma}}{2}, \qquad v_{\text{ac}} = \frac{v_{Pu}^{\Sigma} - v_{Nu}^{\Sigma}}{4},$$

$$R_{\text{dc}} = 2r_d, \qquad L_{\text{dc}} = 2l, \qquad R_{\text{ac}} = \frac{r_d}{2}, \qquad L_{\text{ac}} = \frac{l}{2}.$$

In a mathematical sense, the equations in (13) are the same as those presented in [23], but in this paper, the variables and parameters have their own meanings, because these equations express the model shown in Fig. 2. The differential equations describe four variables: the circulating current, the load current, the voltage sum, and the difference between capacitors in the upper and lower arms. These four variables can provide complete external and internal information about a single phase of the MMC circuit. Therefore, the model shown in Fig. 2 can be taken as an equivalent model of a single phase of the MMC. In Fig. 2, the capacitor voltages C_{dc} and C_{ac} indicate the sum and difference, respectively, of the capacitor voltages of the upper and lower arms. Networks T_1 and T_2 are two ideal transformer models, whose "turn ratios" are controlled by the modulation signal S_u. The dc energy in capacitor C_{dc} is converted to ac and transferred to the load by network T_1, and network T_2 provides another coupling approach between the ac and dc sides. Here, the dc loop can be considered to be the load of the inverter fed by the voltage of capacitor C_{ac}. If there were an initial dc voltage in C_{ac}, it would produce a dc current on the ac side, but at the same time, through network T_2, it would produce a fundamental voltage on the dc side that would induce a fundamental current in the dc loop. In this way, the initial dc energy in C_{ac} can be consumed by the equivalent resistances R_{dc}, R_{ac} and the load resistance, ensuring zero dc energy in C_{ac}.

III. Harmonic Voltage Excitation Model on the DC Side

A. Harmonic Voltage Excitation Model

The model in Fig. 2 shows the interaction between the voltage of capacitor C_{ac} and the circulating current on the dc side through network T_2. The energy in C_{ac} can be released through the dc loop, but at the same time, the current in the dc loop can reappear in another form in C_{ac}. If there is a harmonic voltage in the dc loop, current at the same frequency will be generated through the impedance in the dc loop and can be expressed as follows:

$$i_{Zun} = I_{Zun}\sin(n\omega t + \varphi_n) \tag{14}$$

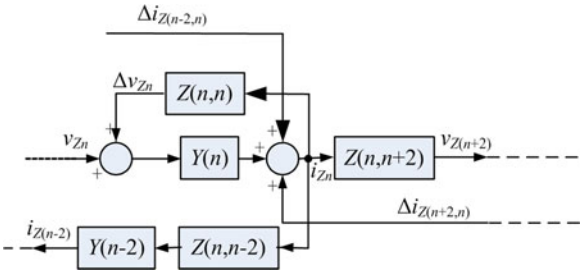

Fig. 3. Harmonic voltage excitation model.

where I_{Zun}, φ_n are the *n*th harmonic current amplitude and phase angle. Through network T_2, this harmonic current produces an incremental voltage in $C_{\rm ac}$

$$\begin{aligned}\Delta v_{\rm acn} = & \frac{m_u I_{Zun}}{(n+1)\omega C_{\rm ac}} \sin\left((n+1)\omega t + \varphi_u + \varphi_n\right) \\ & - \frac{m_u I_{Zun}}{(n-1)\omega C_{\rm ac}} \sin\left((n-1)\omega t - \varphi_u + \varphi_n\right).\end{aligned} \tag{15}$$

This incremental voltage produces another voltage on the dc side through network T_2, which is governed by

$$\begin{aligned}\Delta v_{T1n} = & \; Z\left(n, n+2\right) I_{Zun} \sin\left(\left(n+2\right)\omega t + \varphi_n\right) \\ & + Z\left(n, n\right) I_{Zun} \sin\left(n\omega t + \varphi_n\right) \\ & + Z\left(n, n-2\right) I_{Zun} \sin\left(\left(n-2\right)\omega t + \varphi_n\right)\end{aligned} \tag{16}$$

$$Z(n, n+2) = -j\frac{m_u^2}{(n+1)\omega C_{\rm ac}} \angle 2\varphi_u \tag{17}$$

$$Z(n, n) = j\frac{2nm_u^2}{(n+1)(n-1)\omega C_{\rm ac}} \tag{18}$$

$$Z(n, n-2) = -j\frac{m_u^2}{(n-1)\omega C^{\rm ac}} \angle -2\varphi_u \tag{19}$$

where *Z*(*n*, *n* + 2), *Z*(*n*, *n*), and *Z*(*n*, *n* – 2) are the harmonic voltage impedances that the *n*th circulating harmonic current produces in the (*n* + 2)nd, *n*th, and (*n* – 2)nd harmonic voltages on the dc side through the feedback of $C_{\rm ac}$.

The earlier analysis shows that through network T_2, the *n*th circulating harmonic current would produce new (*n* – 2)nd, *n*th, and (*n* + 2)nd harmonic currents in the circulating current and new (*n* – 1)st and (*n* + 1)st harmonic voltages in $C_{\rm ac}$. At the same time, the new harmonic currents would in turn produce new harmonic currents. This is an endless process illustrated in Fig. 3, where v_{Zn} is the excitation voltage, $\Delta i_{Z(n+2,n)}$ and $\Delta i_{Z(n-2,n)}$ are the *n*th harmonic currents produced by the (*n* + 2)nd and (*n* – 2)nd harmonic currents, respectively, and *Y*(*n*) is the *n*th harmonic admittance, which can be expressed as

$$Y\left(n\right) = R_{\rm dc} + j(n\omega R_{\rm dc} - 1/n\omega C_{\rm dc}). \tag{20}$$

Three factors have been found to produce the corresponding harmonic current: the source voltage v_{Zn}, the *n*th harmonic voltage produced by the (*n* – 2)nd harmonic current, and the *n*th harmonic voltage produced by the (*n* + 2)nd harmonic current. However, the source of these factors is the excitation voltage v_{Zn}. This means that without an excitation voltage, there are no harmonic currents. The harmonic currents are not independent of each other.

B. Generation of Circulating Harmonic Currents in Steady State

The load current can be defined as

$$i_u = I_u \sin(\omega t + \varphi_{Iu}) \tag{21}$$

where i_u is the current amplitude, φ_{Iu} is the load-current phase angle, and $\varphi = \varphi_u - \varphi_I$ is the phase difference between the modulation signal and the load current. If the circulating current is suppressed completely, according to Fig. 2, it is easy to derive the expressions for i_{T11} and v_{T22} using i_u. This is equivalent to the following equation:

$$v_{Z2} = m_{20} I_u \sin(2\omega t + 2\varphi_u + \varphi_{20}) \tag{22}$$

where

$$\tan\varphi_{20} = -\frac{3\sin\varphi}{(3-m_u^2)\cos\varphi}$$

$$m_{20} = \frac{m_u\sqrt{(3-m_u^2)^2\cos^2\varphi + 9\sin^2\varphi}}{16\omega C^{\Sigma}}.$$

When the circulating current is not suppressed, v_{Z2} takes effect in the dc loop and causes interlocking reactions to generate infinite even harmonics in the circulating current and infinite odd harmonic voltages in $C_{\rm ac}$ by the relationships shown in Fig. 3. Ignoring high-order harmonics, each harmonic-current expression can be derived easily, as can the capacitor harmonic voltages, which can be used to analyze the influence of various parameters in the circuit.

IV. Effects of Dead Time and IGBT Voltage Drop

A. Effect of Dead Time

It is assumed in this section that dead time is applied only at the rising edge. Take any submodule as an example; when the upper switch is turned on, the output level is "1," that is, V_C; when the lower switch is turned on, the output level is "0." Fig. 4 shows the dead-time generation principle. In Fig. 4(a) is the single module diagram; (b) and (c) are the control signal waveforms of the upper and lower switches; and (d) and (e) are the output waveforms of the module, where t_D is the dead time.

When $i > 0$, if the lower switch is turned on, current flows through T_L. When the lower switch is turned off, the current will immediately move to the upper antiparallel diode D_U, and capacitor *C* will be connected to the circuit and start to charge. After the dead time, the upper switch is turned on; however, current is still flowing through D_U, which shows that the dead time does not affect the system at this time. When the upper switch is prevented from turning on during the dead time, current

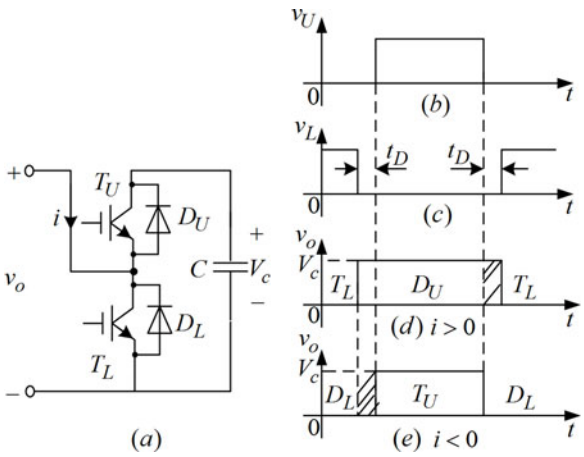

Fig. 4. Dead-time generation schematic.

flows through the upper antiparallel diode D_U until the lower switch is turned on and the current diverted to the lower switch T_L from D_U. Obviously, during dead time, the capacitor is connected into the circuit, which violates the modulation rule and is equivalent to adding a voltage V_C for a duration t_D.

When $i < 0$, if the lower switch is turned on, current flows through the lower antiparallel diode D_L. If the lower switch is cut off, it enters dead time and current flows through D_L until the upper switch is turned on, after which current flows through *C* and T_U and the capacitor is connected into the circuit. Obviously, during dead time, the module output is not in accordance with the modulation rules and is equivalent to reducing the voltage by V_C during t_D. When the upper switch is prevented from turning on, the current through the upper switch immediately drops to zero, and continuously through the lower antiparallel diode D_L, during dead time, the output is zero. After the lower switch is turned on, the current is still continuous through the lower antiparallel diode, and the output voltage is zero. At this point, dead time has no influence on the system.

In conclusion, the effect of dead time is equivalent to a pulse signal in the arm with width t_D and amplitude V_C when the current is greater than zero and $-V_C$ when the current is less than zero. Averaging these pulses produced by dead time during a carrier period, the following equation can be obtained:

$$\Delta v_{td} = V_{td}\text{sign}(i) \tag{23}$$

where

$$V_{td} = \frac{nt_D}{T_C}V_C$$

where *n* is the number of dead-time effects in an arm during a carrier period, T_c is the carrier period, V_c is the dc voltage of the module capacitor, and V_{td} is the amplitude of the equivalent signal caused by the effect of dead time.

B. Effect of IGBT Saturation Voltage Drop

The forward *V–A* characteristics of IGBT when turning on can be described as

$$v = V_{Ton} + ir_{Ton} \tag{24}$$

where V_{Ton} is the IGBT saturation voltage drop and r_{Ton} is the IGBT on-state resistance. The *V–A* characteristics of the antiparallel diode are

$$v = V_{Don} + ir_{Don} \tag{25}$$

where V_{Don} and r_{Don} are, respectively, the voltage drop and the on-state resistance. Considering that r_{Ton} and r_{Don} are commonly smaller, only V_{Ton} and V_{Don} are considered in this paper.

If the system is continuous, at any time in the upper and lower arms, the numbers of "on" modules and "off" modules are $(1 \mp S_u)N/2$ and $(1 \pm S_u)N/2$, respectively. Therefore, the disturbance voltages caused by the saturation-voltage drops in the upper and lower arms can be expressed, respectively, as

$$\Delta v_{\text{TVP}} = V_{\text{TVP}}\text{sign}(i_{Pu}) \tag{26}$$

$$\Delta v_{\text{TVN}} = V_{\text{TVN}}\text{sign}(i_{Nu}) \tag{27}$$

where

$$V_{\text{TVP}} = \frac{V_{Ton}+V_{Don}}{2}N + \frac{V_{Ton}-V_{Don}}{2}NS_u\text{sign}(i_{Pu})$$

$$V_{\text{TVN}} = \frac{V_{Ton}+V_{Don}}{2}N - \frac{V_{Ton}-V_{Don}}{2}NS_u\text{sign}(i_{Nu}).$$

C. Combined Effects of Dead Time and IGBT Voltage Drop

The disturbance voltages caused by the dead time and the saturation voltage drop can be integrated as

$$\Delta v_{tvP} = (V_{td} + V_{\text{TVP}})\text{sign}(i_{Pu}) \tag{28}$$

$$\Delta v_{tvN} = (V_{td} + V_{\text{TVN}})\text{sign}(i_{Nu}) \tag{29}$$

where V_{td}, V_{TVP}, and V_{TVN} are defined in (23), (26), and (27), respectively.

Therefore, the disturbance voltage is a rectangular wave whose duty cycle ratio is determined by the polarity of the arm current. The generation principle of the effects of DTVD is shown in Fig. 5(a) shows the current waves for the upper and lower arms. In this case, the harmonic components are ignored, and only the dc and the fundamental components are retained. The waveforms of Δv_{tvP} and Δv_{tvN} (ignoring the amplitude fluctuation), which are rectangular waves, are shown in Fig. 5(b) and (c), respectively. Fig. 5(d) shows the difference between Δv_{tvN} and Δv_{tvP}, which indicates the effect of DTVD upon the output voltage. The waveform of the sum of Δv_{tvP} and Δv_{tvN} is shown in Fig. 5(e), which reflects the DTVD on the dc side. From Fig. 5, it can be seen that the DTVD will produce a unipolar double fundamental frequency pulse on the dc side of the system, which obviously causes even-order harmonics, especially second order, in the circulating current and affects the dc capacitor voltage. At the same time, DTVD can produce a rectangular fundamental wave in the output and will affect the amplitude and THD of the output voltage. The disturbance voltages due to DTVD on the ac and dc sides of the system can be described as

$$\Delta v_{\text{ac}} = \frac{\Delta v_{tvN} - \Delta v_{tvP}}{2} \tag{30}$$

$$\Delta v_{\text{dc}} = \Delta v_{tvN} + \Delta v_{tvP} \tag{31}$$

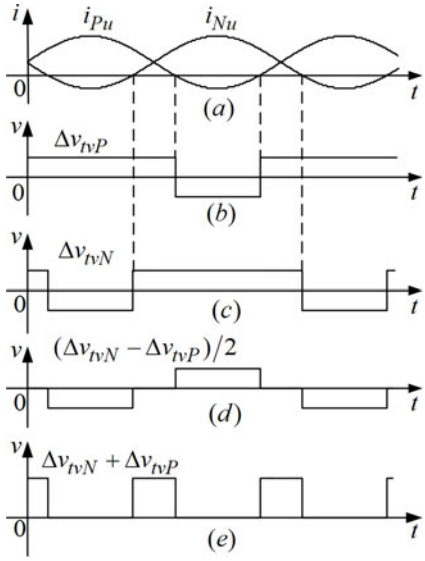

Fig. 5. Effects of DTVD on the ac and dc sides of the system.

D. Impact on Circulating Harmonic Currents by DTVD

The analysis described in Section IV indicates that the effects of DTVD add a fundamental frequency rectangular wave to the output voltage that causes some harmonics in the output; at the same time, they produce a single-polarity double-frequency pulse on the dc side. Ignoring the harmonics in the arm currents, the width of $\Delta v_{\rm dc}$ can be expressed as

$$\tau = 2\arcsin\left(\frac{1}{4}m_u\cos\varphi\right). \tag{32}$$

When an MMC operates in an inverting state, the single-polarity pulse is positive, which decreases the average capacitor voltage and produces circulating harmonic currents. Removing the dc component of $\Delta v_{\rm dc}$ and keeping an ac pulse on the dc side, as described in Section III, produces infinite even harmonic currents on the dc side. Ignoring other-order harmonics produced by the harmonic excitation voltage, any harmonics in $\Delta v_{\rm dc}$ produce the same frequency of harmonic current, which can be derived as

$$i_{Zn} = \frac{v_{Zn}}{Z(n) - Z(n,n)} \tag{33}$$

where $Z(n) = 1/Y(n)$ is the impedance of the dc loop. According to (18), the denominator of the right-hand side in (33) can be expressed as

$$Z'(n) = R_{\rm dc} + jn\omega L_{\rm dc} - j\frac{1}{n\omega C^n_{\rm dc}} \tag{34}$$

where

$$C^n_{\rm dc} = C_{\rm dc} + \frac{(n+1)(n-1)}{2n^2m_u^2}C_{\rm ac}.$$

Obviously, for the *n*th harmonic voltage in the dc loop, if other-order harmonics are ignored, the dc loop can be considered equivalent to a second-order circuit composed of a capacitor, an inductor, and a resistor, as shown in Fig. 6. The capacitance varies with harmonic frequency within a certain range. If the imaginary part of (34) is zero, resonance oscillation will occur in the dc loop, as verified in [14].

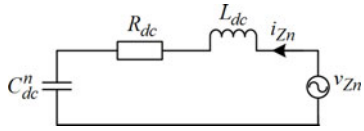

Fig. 6. Equivalent circuit for the voltage caused by DTVD on the dc side.

Therefore, the circulating current produced by the pulse depending on the effects of DTVD can be obtained from Fig. 6. In a practical MMC system, the capacitance is generally relatively large. Inductance plays a leading role, forming a sawtooth wave in the circulating current.

However, if there are circulating harmonic currents, the zero-crossing point of the arm currents will change, and so will the pulse width $\Delta v_{\rm dc}$. Analysis indicates that when the circulating harmonic current amplitude is much smaller than that of the load current, $\Delta v_{\rm dc}$ is still a single-polarity pulse signal, but its width becomes larger, which will increase the impact of DTVD. If the circulating harmonic amplitude is the same as or higher than that of the load current, a double-polarity rectangular wave with double fundamental frequency will appear, and the effects of DTVD will become more apparent.

The amplitude of $\Delta v_{\rm dc}$ can be shown to be independent of the output current and voltage and to depend only on DTVD. Therefore, the value of the circulating harmonic currents caused by DTVD is limited within a range. When the circulating harmonic currents caused by the output current are far outside this range, the currents caused by DTVD can be ignored.

V. Circulating Harmonic Current Suppression Under the Influence of DTVD

A. Circulating Current Control Model

To control the circulating current, a control signal is added to the modulation signals of the upper and lower arms, and (9) and (10) can be revised as

$$v_{Pu} = \frac{1 - S_u + d}{2}v^{\Sigma}_{Pu} \tag{35}$$

$$v_{Nu} = \frac{1 + S_u + d}{2}v^{\Sigma}_{Nu} \tag{36}$$

where *d* is the control variable. The control matrix can then be modified as

$$\mathbf{A_d} = \begin{bmatrix} -R_{\rm dc} & 0 & -(1+d) & 2S_u \\ 0 & -R_{\rm ac} & \frac{1}{2}S_u & -(1+d) \\ (1+d) & -\frac{1}{2}S_u & 0 & 0 \\ -2S_u & (1+d) & 0 & 0 \end{bmatrix}. \tag{37}$$

The equivalent model shown in Fig. 2 can be revised into the circulating current control model shown in Fig. 7. Circulation control produces a voltage on the dc side to control the

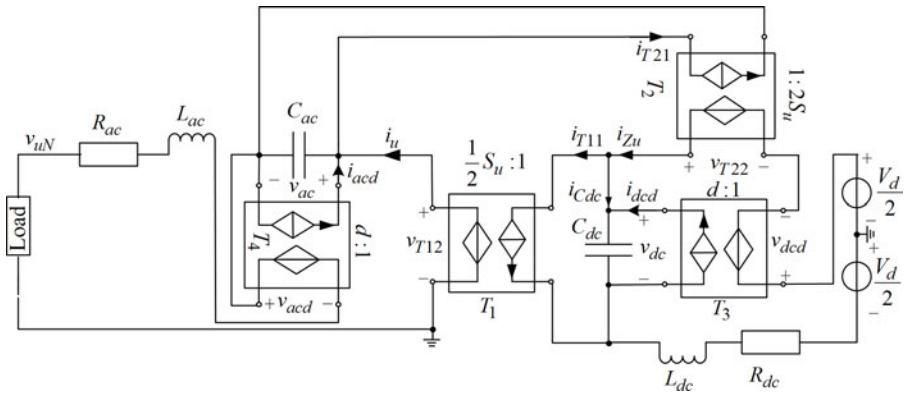

Fig. 7. Circulating current control equivalent model of the MMC.

circulating current through the ideal transform network T_3 with a "turn ratio" of d. However, at the same time, capacitor $C_{\rm ac}$ causes a parasitic voltage on the ac side through network T_4.

B. Circulating Harmonic Current Suppression Strategy

The earlier analysis indicates that the circulating harmonic currents are the incentive products of v_{Z2} caused by the output current and $\Delta v_{\rm dc}$ caused by DTVD exciting the dc loop of the MMC. Therefore, suppression of circulating harmonic currents can be achieved by cancelling v_{Z2} and $\Delta v_{\rm dc}$. To eliminate the circulating harmonic currents caused by the output current, it is necessary only to apply a reverse voltage to v_{Z2} on the dc side, not to design an independent controller for every harmonic current as proposed in [25].

Let

$$v_{\rm dcd} = -v_{Z2}. \tag{38}$$

Then

$$d = \frac{v_{\rm dcd}}{v_{\rm dc}} \approx \frac{v_{\rm dcd}}{V_d}. \tag{39}$$

This is an open-loop control strategy. Although this strategy comes from the idea of cancelling the effects of the produced circulating current, it is still an open-loop strategy and results in circulating currents without harmonics so that it has a consistent physical nature with the strategy proposed in [19]–[21]. However, the system proposed here does not attempt to control capacitor energy and does not depend on the equivalent resistance in the arm.

The frequency of the control variable d is twice the fundamental frequency, as is the "turn ratio" frequency. Fig. 7 shows that the dc component in the circulating current will inject a new second-harmonic current into capacitor $C_{\rm dc}$ through network T_3 to produce a new second-harmonic voltage and a new circulating harmonic current. The load current i_u will inject new fundamental and third harmonic currents into $C_{\rm ac}$ through T_4 to produce new fundamental and third-harmonic voltages, and these new voltages will also produce a new even-harmonic circulating current through network T_2.

It is apparent that the circulating harmonic current cannot be completely eliminated. However, thanks to the smaller value of the control variable d, the voltages produced by the injecting currents to $C_{\rm dc}$ and $C_{\rm ac}$ by $i_{\rm Zu}$ and i_u through networks T_3 and T_4, respectively, are relatively smaller and can be ignored.

To eliminate the impact of DTVD, the polarities of the arm currents will first be detected and Δv_{tvP} and Δv_{tvN} calculated, that is, the voltage effects of DTVD in the arms. Therefore

$$d_{tvP} = -\frac{\Delta v_{tvP}}{V_d} \tag{40}$$

$$d_{tvN} = -\frac{\Delta v_{tvN}}{V_d} \tag{41}$$

d_{tvP} and d_{tvN} are then added to the modulation signals of the upper and lower arms, respectively, to produce control voltages in the arms to counteract the voltage effects of DTVD.

TABLE I
SIMULATION AND EXPERIMENTAL PARAMETERS

Parameters	Quantities for Simulation	Quantities for Experiment
Capacitance per module	4700 μF	2200 μF
Inductance in arm	6 mH	3 mH
DC equivalent resistance	0.5 Ω	
Load inductance	0	25 mH
Load resistance	70 Ω	22 Ω
Modules per arm	14	4
Amplitude modulation rate	0.9	0.9
Average submodule switching frequency	0.357 kHz	1.25 kHz
Input dc voltage	14 kV	560 V
Output frequency	50 Hz	50 Hz
Dead time	3 μS	3 μS
IGBT voltage drop	3 V	About 3 V

VI. SIMULATED AND EXPERIMENTAL RESULTS

To verify the analysis, a simulation platform with 14 modules per arm and a downscaled experimental platform with four modules per arm were constructed; their detailed parameters are shown in Table I. The simulation platform was used to study the impact of DTVD on the system, and the experimental platform enabled research into harmonic voltage excitation on the dc side and circulating harmonic current suppression.

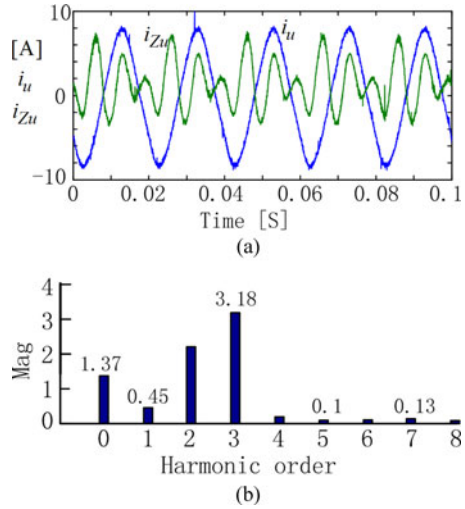

Fig. 8. Experimental waveforms of the output and circulating currents after injecting a third harmonic voltage on the dc side. (a) Waveforms of the output and circulating currents. (b) Spectral analysis diagram of the circulating current.

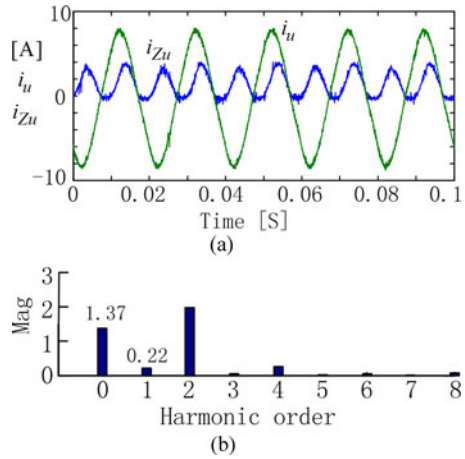

Fig. 9. Experimental waveforms of the output and circulating currents before injecting the third harmonic voltage on the dc side. (a) Waveforms of the output and circulating currents. (b) Spectral analysis diagram of the circulating current.

A. Experimental Study of Harmonic Voltage Excitation on the DC Side

To study harmonic variation when injecting a harmonic voltage into the dc side, a third harmonic signal equal to 0.05sin3ωt was added to the modulation signals in both the upper and lower arms, with which a third harmonic voltage on the dc side was produced. According to the analysis in Section III, this signal should produce odd harmonic currents in the circulating current and even harmonic voltages and a dc voltage in $C_{\rm ac}$.

Figs. 8 and 9 show the experimental waveforms of the output current and the circulating current after and before injecting the third harmonic voltage on the dc side, where Fig. 8(a) shows the experimental waveforms and Fig. 8(b) shows the harmonic component analysis. It is apparent that after injecting the third harmonic voltage, the output current did not change. As for the circulating current, besides the significantly increased third harmonic, the fundamental, the fifth, and the seventh harmonics were increased at the same time, which indicates that the third harmonic voltage produces new circulating odd harmonic currents.

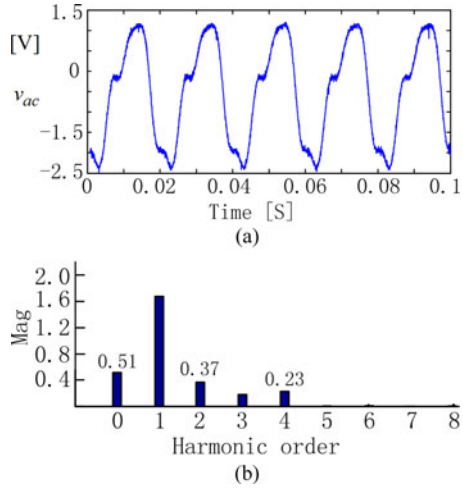

Fig. 10. Experimental waveforms of $v_{\rm ac}$ after injecting the third harmonic voltage. (a) Waveforms of $v_{\rm ac}$. (b) Spectral analysis diagram of $v_{\rm ac}$.

Figs. 10 and 11 show the waveforms and the harmonic component analysis on $v_{\rm ac}$ after and before injecting the third voltage. After injecting the third harmonic voltage, the dc component of $v_{\rm ac}$ changed from about $\pm$0.25 V to about –0.5 V, a decrease of about 0.75 V. The difference in capacitor voltage between the upper and lower arms was about 3 V. In addition, the second and the fourth harmonics in $v_{\rm ac}$ were clearly changed.

Note that before injecting this third harmonic, there was still a dc component of about 0.25 V in $v_{\rm ac}$ (although it was very small) because the system parameters were not absolutely symmetrical, an issue which will be addressed in future work. However, beside this dc component, there were a few even harmonics in $v_{\rm ac}$ and fundamental and other odd harmonics in the circulating current i_{Zu}. This suggests that the dc component cannot exist alone without other even harmonics in $v_{\rm ac}$ and other odd harmonics in i_{Zu} because the circulating harmonic currents and harmonic voltages in $v_{\rm ac}$ have a causal relationship and influence each other.

B. Simulation Study on the Impact of DTVD

To verify the impact of DTVD, a simulation study was conducted using the parameters listed in Table I. The simulation waveforms are shown in Figs. 12–14, where (a) shows the waveforms including DTVD and (b) shows the waveforms with ideal power devices and a dead time of zero.

Fig. 12 shows the waveforms of the arm currents, and Fig. 13 shows the waveforms of the output and circulating currents. Comparing (a) and (b) in Figs. 12 and 13, it is apparent that under the influence of DTVD, the amplitude of the circulating current is reduced, and the shape of the arm currents is obviously changed. Fig. 12(c) shows the difference between the waves

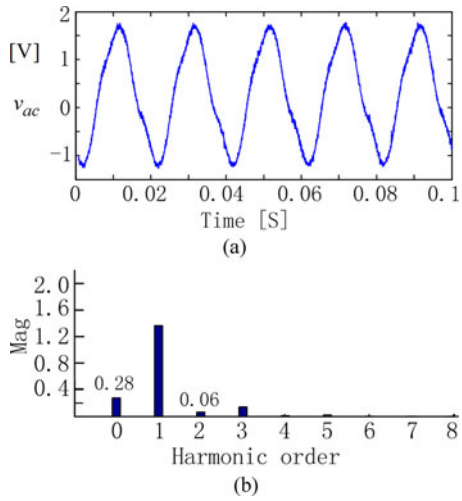

Fig. 11. Experimental waveforms of $v_{\rm ac}$ before injecting the third harmonic voltage. (a) Waveforms of $v_{\rm ac}$. (b) Spectral analysis diagram of $v_{\rm ac}$.

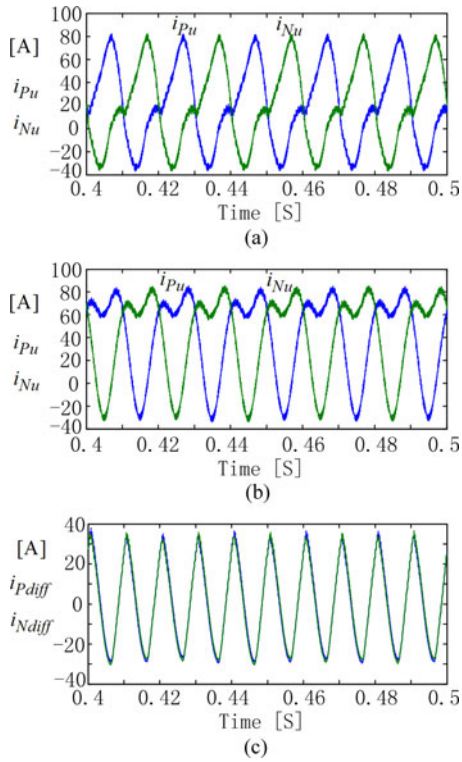

Fig. 12. Simulated waveforms of arm currents with and without DTVD. (a) Arm currents with DTVD. (b) Arm currents without DTVD. (c) Difference between arm currents with and without DTVD.

shown in (b) and (a) and referred to as $i_{\rm Pdiff}$ and $i_{\rm Ndiff}$, which indicates the contribution of DTVD to the circulating current. This waveform is similar to a double-frequency sawtooth wave with a peak-to-peak value greater than 70 A, which is even larger than that caused by the output current. In Fig. 12(c), there is a small dc component in the wave, which indicates that under the influence of DTVD, the dc component in the circulating current decreases a little, or the output power decreases.

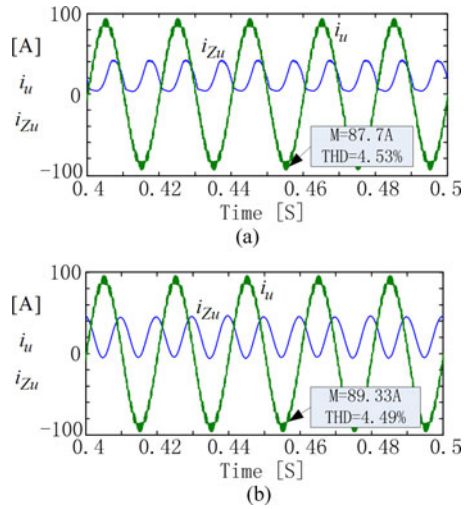

Fig. 13. Simulated waveforms of output and circulating currents with and without DTVD. (a) Output and circulating currents with DTVD. (b) Output and circulating currents without DTVD.

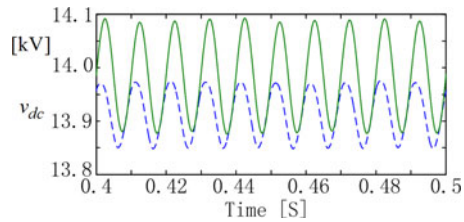

Fig. 14. Simulated $v_{\rm dc}$ waveforms with and without DTVD (solid line: without DTVD, dotted line: with DTVD).

Fast Fourier transform (FFT) analysis of the output currents shown in Fig. 13(a) and (b) indicates that the amplitude of the fundamental current is 87.7 A and the total harmonic distortion (THD) is 4.53%. However, the same components shown in Fig. 13(b) are 89.33 A and 4.49%, respectively. In other words, under the influence of DTVD, the output current decreases a little and the THD increases a little.

Fig. 14 shows the waveforms of $v_{\rm dc}$, where the solid-line waveform represents the simulation without DTVD and the dotted-line waveform that with DTVD. Under the influence of DTVD, the average capacitor voltage decreased by 75 V, slightly decreasing the output current and the dc component of the circulating current. However, the peak-to-peak value of the capacitor voltage fluctuation decreased from 210 to 120 V, indicating obvious suppression.

C. Experimental Study on Circulating Harmonic Current Suppression

The downscaled experimental platform was used to verify further the impact of DTVD and the circulating harmonic current suppression strategy. The experimental waveforms for output and circulating currents without circulating harmonic currents suppression are shown in Fig. 12(b). Fig. 15(a) shows the

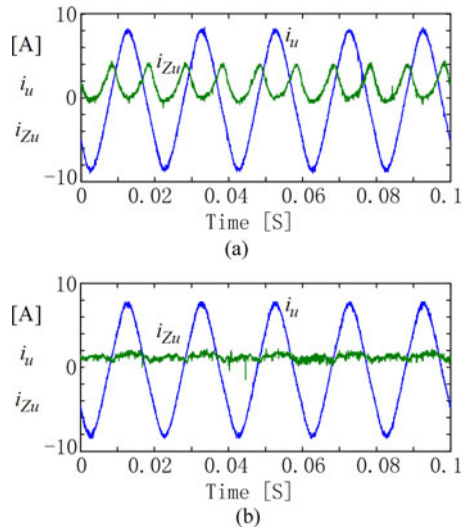

Fig. 15. Experimental waveforms for output and circulating currents with the proposed circulating harmonic current suppression strategy. (a) Waveforms with suppression only of circulating harmonic currents caused by the output current. (b) Waveforms with suppression of circulating harmonic currents caused both by the output current and by DTVD.

waveforms of the output and circulating currents with the open-loop suppression strategy proposed in (38), which suppresses only the circulating harmonic currents produced by the output current and does nothing to DTVD. Compared to Fig. 12(b), it is clear that the circulating harmonic currents are still large and cannot be suppressed.

Fig. 15(b) shows the waveforms with suppression of the circulating harmonic currents caused by both output current and DTVD, which shows a satisfactory result.

VII. Conclusion

In this paper, a method for analyzing and suppressing circulating harmonic currents considering DTVD is presented. It has been found that if the output current is not very high, the circulating harmonic currents caused by DTVD cannot be ignored. With DTVD, the THD in the output increases slightly, and in an inverting state, the capacitor voltage decreases. The circulating harmonic currents are produced by the voltages on the dc side. These voltages are produced by the output current and the DTVD in steady state without circulating current control. Therefore, circulating harmonic current suppression can be achieved by eliminating the voltages that producing these harmonic currents. A nth harmonic voltage on the dc side will produce $n \pm 2k(k = 0, 1, 2, \ldots)$ order harmonics in the circulating current and $(n + 2k + 1)$-order harmonics in the capacitor voltage difference in the upper and lower arms. If n is an odd number, the harmonic will produce a dc component in the capacitor voltage difference. The model, strategy, and conclusions can be used to analyze and control the circulating current and the capacitor voltages.

References

[1] M. Malinowski, K. Gopakumar, J. Rodrigue, and M. A. Pérez, "A survey on cascaded multilevel inverters," *IEEE Trans. Ind. Electron.*, vol. 57, no. 7, pp. 2197–2207, Jul. 2010.

[2] H. Akagi, "Classification, terminology, and application of the modular multilevel cascade converter (MMCC)," *IEEE Trans. Power Electron.*, vol. 26, no. 11, pp. 3119–3130, Nov. 2011.

[3] S. Kouro, M. Malinowski, and K. Gopakumar, "Recent advances and industrial applications of multilevel converters," *IEEE Trans. Ind. Electron.*, vol. 57, no. 8, pp. 2553–2580, Aug. 2010.

[4] M. Saeedifard and R. Iravani, "Dynamic performance of a modular multilevel back-to-back HVDC system," *IEEE Trans. Power Del.*, vol. 25, no. 4, pp. 2903–2912, Oct. 2010.

[5] H. P. Mohammadi and M. Tavakoli Bina, "A transformerless medium-voltage STATCOM topology based on extended modular multilevel converters," *IEEE Trans. Power Electron.*, vol. 26, no. 5, pp. 1534–1545, May 2011.

[6] J. Rodriguez, G. Franquelo, S. Kouro, I. Leon, C. Portillo, M. Prats and A. Perez, "Multilevel converters: An enabling technology for high-power applications," *Proc. IEEE*, vol. 97, no. 11, pp. 1786–1817, Nov. 2009.

[7] N. Flourentzou, V. G. Agelidis, and G. D. Demetriades, "VSC-based HVDC power transmission systems: An overview," *IEEE Trans. Power Electron.*, vol. 24, no. 3, pp. 592–602, Jul. 2009.

[8] A. Lesnicar and R. Marquardt, "An innovative modular multilevel converter topology suitable for a wide power range," in *Proc. IEEE 2003 PowerTech Conf.*, Bologna, Italy, Jun. 2003, pp. 23–26.

[9] M. Hagiwara, K. Nishimura, and H. Akagi, "A medium-voltage motor drive with a modular multilevel PWM inverter," *IEEE Trans. Power Electron.*, vol. 25, no. 7, pp. 1786–1799, Jul. 2010.

[10] M. Winkelnkemper, A. Korn, and P. Steimer, "A modular direct converter for transformerless rail interties," in *Proc. IEEE Int. Ind. Electron. Symp.*, 2010, pp. 562–567.

[11] K. Ilves, A. Antonopoulos, S. Norrga, and H.-P. Nee, "Steady-state analysis of interaction between harmonic components of arm and line quantities of modular multilevel converters," *IEEE Trans. Power Electron.*, vol. 27, no. 1, pp. 57–68, Jan. 2012.

[12] Q. Song, W. Liu, X. Li, H. Rao, S. Xu, and L. Li, "A steady-state analysis method for a modular multilevel converter," *IEEE Trans. Power Electron.*, vol. 28, no. 8, pp. 3702–3713, Aug. 2013.

[13] N. Ahmed, L. Ängquist, S. Norrga, and H.-P. Nee, "Validation of the continuous model of modular multilevel converter with blocking/deblocking capacity," in *Proc. 10th IET Int. Conf. AC DC Power Transmiss.*, Dec. 2012, pp. 4–6.

[14] N. Ahmed, L. Ängquist, and H.-P. Nee, "Continuous modeling of open-loop control based negative sequence current control of modular multilevel converters for HVDC transmission," in *Proc. EPE ECCE Eur.*, Lille, France, Sep. 2013, pp. 3–5.

[15] S. Norrga, L. Ängquist, K. Ilves, L. Harnefors, and H.-P. Nee, "Frequency-domain modeling of modular multilevel converters—With application to maximizing the operating region," in *Proc. of 38th Ann. Conf. 2012 IEEE Ind. Electron. Society*, Oct. 25–28, 2012, Montreal, QC, Canada, pp. 4967–4972.

[16] S. Norrga, L. Ängquist, K. Ilves, L. Harnefors, and H.-P. Nee, "Decoupled steady-state model of the modular multilevel converter with half-bridge cells," presented at the IET Power Electron., Mach. Drives Conf., Bristol, U.K., Mar. 27–29, 2012.

[17] M. Hagiwara, R. Maeda, and H. Akagi, "Control and analysis of the modular multilevel cascade converter based on double-star chopper-cells (MMCC-DSCC)," *IEEE Trans. Power Electron.*, vol. 26, no. 6, pp. 1649–1658, Jun. 2011.

[18] Makoto Hagiwara and Hirofumi Akagi, "Control and experiment of pulsewidth-modulated modular multilevel converters," *IEEE Trans. Power Electron.*, vol. 24, no. 7, pp. 1737–1746, Jul. 2009.

[19] L. Angquist, A. Antonopoulos, D. Siemaszko, K. Ilves, M. Vasiladiotis, and H.-P. Nee, "Inner control of modular multilevel converters—An approach using open-loop estimation of stored energy," presented at the Int. Power Electron. Conf., Sapporo, Japan, Jun. 21–24, 2010.

[20] L. Angquist, A. Antonopoulos, D. Siemaszko, K. Ilves, M. Vasiladiotis, and H.-P. Nee, "Open-loop control of modular multilevel converters using estimation of stored energy," *IEEE Trans. Ind. Appl.*, vol. 47, no. 6, pp. 2516–2524, Nov./Dec. 2011.

[21] D. Siemaszko, A. Antonopoulos, K. Ilves, M. Vasiladiotis, L. Angquist, and H.-P. Nee, "Evaluation of control and modulation methods for modular multilevel converters," in *Proc. IPEC*, 2010, pp.746–753.

[22] Z. Li, P. Wang, Z. Chu, H. Zhu, Y. Luo, and Y. Li, "An inner current suppressing method for modular multilevel converters," *IEEE Trans. Power Electron.*, vol. 28, no. 11, pp. 4873–4879, Nov. 2013.
[23] L. Harnefors, A. Antonopoulos, S. Norrga, L. Ängquist, and H.-P. Nee, "Dynamic analysis of modular multilevel converters," *IEEE Trans. Ind. Electron.*, vol. 60, no. 7, pp. 2526–2537, Jul. 2013.
[24] L. Harnefors, A. Antonopoulos, and H.-P. Nee, "Global stability of modular multilevel converters with measurement lag and circulating-current control," in *Proc. of EPE ECCE-Eur.*, Lille, Sep. 2013, pp. 3–5.
[25] Z. Li, Y. Li, P. Wang, H. Zhu, Z. Chu, and S. Wang, "Improving the performance of modular multilevel converter by reducing the dead time effect," in *Proc. EPE*, 2011, pp. 1–10.

Baichao Chen (M'99) received the B.Sc. degree in electrical engineering from Huazhong University of Science and Technology, Wuhan, China, in 1982, and the M.Sc. and Ph.D. degrees from the College of Electrical Engineering, Wuhan University, Wuhan, in 1986 and 1993, respectively.

From 1998 to 1999, he was a Visiting Researcher with the Department of Electrical, Computer, and Systems Engineering, Rensselaer Polytechnic Institute, Troy, NY, USA. He is currently a Professor of Electrical Engineering with the College of Electrical Engineering, Wuhan University. His current research interests include hig-voltage engineering, power quality, and power electronic applications in high-voltage engineering.

Yaojun Chen was born on February 28, 1977. He received the B.S. and M.S. degrees from the Wuhan Electronic Information Institute, Wuhan, China, in 2000 and 2005, respectively. He is currently working toward the Ph.D. degree in the School of Electrical Engineering, Wuhan University, Wuhan, China.

He is currently a Lecturer with Wuhan Electronic Information Institute, Wuhan. He is currently involved in the theoretical research and applications of the modular multilevel converters. His current research interests include power quality and inverter control.

Cuihua Tian received the B.Sc., M.Sc., and Ph.D. degrees from the College of Electrical Engineering, Wuhan University, Wuhan, China, in 1992, 1997, and 2005, respectively.

She is currently an Associate Professor of Electrical Engineering with the College of Electrical Engineering, Wuhan University. Her current research interests include high-voltage engineering, power quality, and microcomputer-based control systems.

Jiaxin Yuan (M'05) was born in Nanchang, China, on June 10, 1981. He received the B.S. and Ph.D. degrees from the School of Electrical Engineering, Wuhan University, Wuhan, China, in 2002 and 2007, respectively.

From 2007 to 2009, he was a Lecturer with Wuhan University, where he was involved in research and development of STATCOM and DSP inverter control. In 2010, he became an Associate Professor in the School of Electrical Engineering, Wuhan University, where he was involved in power electronics system control, power quality issues, and application and control of inverters. He is currently a Visiting Scholar at the Electrical and Computer Engineering, Ohio State University, Columbus, USA.

Xiu Yao (S'10) received the B.S. and M.S. degrees from Xi'an Jiaotong University, Xian, China, in 2007 and 2010, respectively. She is currently working toward the Ph.D. degree with the Ohio State University, Columbus, OH, USA.

Her current research interests include dc arc fault detection in high-voltage and power electronic systems, harmonic elimination of multilevel inverter, and the utilization of modular multilevel converter in high-power systems.